*Am J Physiol Cell Physiol* 288: C523–C534, 2005.
First published November 10, 2004; doi:10.1152/ajpcell.00448.2003.

# Kinetics, molecular basis, and differentiation of L-lactate transport in spermatogenic cells

**Sebastian Brauchi,[1] Maria C. Rauch,[2] Ivan E. Alfaro,[1] Christian Cea,[1] Ilona I. Concha,[2] Dale J. Benos,[3] and Juan G. Reyes[1,3]**

[1]*Instituto de Química, Pontificia Universidad Católica de Valparaíso, Valparaíso;* [2]*Instituto de Bioquímica, Universidad Austral de Chile, Valdivia, Chile; and* [3]*Department of Physiology and Biophysics, University of Alabama at Birmingham, Birmingham, Alabama*

Submitted 16 October 2003; accepted in final form 5 November 2004

**Brauchi, Sebastian, Maria C. Rauch, Ivan E. Alfaro, Christian Cea, Ilona I. Concha, Dale J. Benos, and Juan G. Reyes.** Kinetics, molecular basis, and differentiation of L-lactate transport in spermatogenic cells. *Am J Physiol Cell Physiol* 288: C523–C534, 2005. First published November 10, 2004; doi:10.1152/ajpcell.00448.2003.—Round spermatid energy metabolism is closely dependent on the presence of L-lactate in the external medium. This L-lactate has been proposed to be supplied by Sertoli cells in the seminiferous tubules. L-Lactate, in conjunction with glucose, modulates intracellular $Ca^{2+}$ concentration in round spermatids and pachytene spermatocytes. In spite of this central role of L-lactate in spermatogenic cell physiology, the mechanism of L-lactate transport, as well as possible differentiation during spermatogenesis, has not been studied in these cells. By measuring radioactive L-lactate transport and intracellular pH ($pH_i$) changes with $pH_i$ fluorescent probes, we show that these cells transport L-lactate using monocarboxylate-$H^+$ transport (MCT) systems. RT-PCR, in situ mRNA hybridization, and immunocyto- and immunohistochemistry data show that pachytene spermatocytes express mainly the MCT1 and MCT4 isoforms of the transporter (intermediate- and low-affinity transporters, respectively), while round spermatids, besides MCT1 and MCT4, also show expression of the MCT2 isoform (high-affinity transporter). These molecular data are consistent with the kinetic data of L-lactate transport in these cells demonstrating at least two transport components for L-lactate. These separate transport components reflect the ability of these cells to switch between the generation of glycolytic L-lactate in the presence of external glucose and the use of L-lactate when this substrate is available in the external environment. The supply of these substrates is regulated by the hormonal control of Sertoli cell glycolytic activity.

cell differentiation; seminiferous tubules; spermatogenesis; testicle; meiosis

SPERMATOGENESIS IS A COMPLEX PHYSIOLOGICAL PROCESS that involves cell proliferation, meiotic division, and a final differentiation of postmeiotic cells into spermatozoa. In mammals, this process occurs under the influence of Sertoli cells, which are the sustentacular epithelial cells in the seminiferous tubules. The mechanisms by which Sertoli cells control the spermatogenic process are not known, but the present view is that control of this process is accomplished through receptor-mediated cell-cell contacts and molecules secreted by Sertoli cells into the adluminal compartment in the seminiferous tubules (see, e.g., Ref. 16). Some of these Sertoli cell-spermatogenic cell interactions are hypothesized to take place through release and uptake of metabolic substrates in the seminiferous tubules. Thus it has been proposed that Sertoli cells "nurse" spermatogenic cells by releasing L-lactate as an end product of their glycolytic metabolism (14, 18, 21, 35). In the adluminal compartment, this compound is thought to be taken up and metabolized by meiotic and postmeiotic spermatogenic cell mitochondria (17, 21). Glucose can cross the hematotesticular barrier (40) and be taken up by the spermatogenic cells (24), because it is a glycolytic substrate of meiotic and postmeiotic spermatogenic cells (1, 12, 21–23). In round spermatids, external L-lactate is an efficient metabolite for oxidative metabolism in these cells. L-Lactate produced during glycolysis is mainly excreted toward the external medium, with little channeling into oxidative metabolism (21, 22). Hence, external and internal L-lactate are handled differently by spermatogenic cells, especially by round spermatids. This characteristic of spermatid L-lactate metabolism is part of a general differentiation of carbohydrate metabolism that takes place in spermatogenic cells (see, e.g., Ref. 1). In this metabolic differentiation process, postmeiotic spermatogenic cells (e.g., spermatids), but not meiotic spermatogenic cells (e.g., pachytene spermatocytes), respond to D-glucose with an increased turnover of adenine nucleotides, resulting in a decrease in total ATP concentration and an increase in AMP concentrations in these cells (12, 21, 22, 32). We recently demonstrated that this metabolic differentiation has physiological implications, conferring on these cells the ability to respond with an increase in intracellular calcium concentration ($[Ca^{2+}]_i$) subsequent to a rise of D-glucose concentration in the external medium (15, 32). L-Lactate can decrease this glucose-induced increase in $[Ca^{2+}]_i$ in round spermatids. A Sertoli cell-spermatogenic cell interaction model has been proposed (32) in which, through transport and glycolytic properties, Sertoli cells control the passage or production of metabolic substrates (glucose and L-lactate) toward the adluminal compartment. In this compartment, the transport and metabolism of L-lactate and D-glucose by spermatogenic cells are thought to determine their intracellular levels of adenine nucleotides (ATP, ADP, and AMP) as well as the activities of $Ca^{2+}$ and $H^+$ transport ATPases and hence their $[Ca^{2+}]_i$ and $pH_i$. The fact that two possible sources of L-lactate (endogenous and exogenous) are handled by meiotic and postmeiotic spermatogenic cells strongly suggests that different L-lactate transport systems may be expressed in these cells. Although many of the energy metabolic properties of pachytene spermatocytes and round spermatids have been

Address for reprint requests and other correspondence: J. G. Reyes, Instituto de Química, Pontificia Universidad Católica de Valparaíso, Casilla 4059, Valparaíso, Chile (E-mail: jreyes@ucv.cl).

The costs of publication of this article were defrayed in part by the payment of page charges. The article must therefore be hereby marked "*advertisement*" in accordance with 18 U.S.C. Section 1734 solely to indicate this fact.

  

characterized (1, 12, 15, 22, 32, 33), the differentiation and molecular and kinetic properties of L-lactate transport in spermatogenic cells are not known. A family of monocarboxylate transporters (MCT) that present a monocarboxylate-$H^+$ cotransport mechanism (13) undertake L-lactate transport in mammalian cells. Four isoforms of MCT have been described in rodents. MCT1, MCT2, and MCT4 have a wide tissue distribution. In contrast, the MCT3 isoform is expressed mainly in the retina. The $K_m$ for L-lactate of the different isoforms ranges from 0.5 mM for MCT2 to 10–22 mM for MCT4. The MCT1 isoform has intermediate $K_m$ values of ~3.5–7 mM (7, 9, 13). The expression of different MCT isoforms has been demonstrated to be regulated by contractile activity in muscle (4), showing the ability of this system to adapt to different physiological requirements of the cells. Recently, Boussuar et al. (6) and Goddard et al. (11) reported the expression of MCT1 and MCT2 in mouse spermatogenic cells.

In this study, we have explored the hypothesis that both high- and low-affinity isoforms of L-lactate transporters are expressed and functional in spermatogenic cells and that MCT isoform expression changes during spermatogenesis.

## MATERIALS AND METHODS

### *Rat Spermatogenic Cell Preparation*

Rat spermatogenic cell populations were prepared from the testicles of adult Sprague-Dawley rats (50–70 days old) as described by Romrell et al. (36). Rats were housed with free access to food and water using a 12:12-h light-dark cycle. The animals were lightly narcotized by exposure to $CO_2$ for 45 s and then killed by cervical dislocation. A 95% $O_2$-5% $CO_2$ atmosphere was maintained throughout the tissue enzymatic digestion procedure. The pachytene spermatocyte (85 ± 5% purity) and round spermatid fractions (92 ± 4% purity) were identified by their size as well as by the typical aspect of the nucleus stained with Hoechst H33342 (Molecular Probes, Eugene, OR) (31). The round spermatid fraction contained cells between stages 1 and 7. Our method of vital cell identification did not allow a further classification of rat spermatids at these stages of development. The isolated cells were used within 4 h after the purification procedures. All animal experimentation was conducted in accordance with the American Physiological Society's "Guiding Principles for Research Involving Animals and Humans," and all animal protocols were reviewed and approved by the Institutional Animal Care and Use Committee of each university.

### *RNA Purification*

Total RNA was obtained from 1 million purified spermatogenic cells using a Stratagene Absolutely RNA Miniprep RT-PCR kit (Stratagene, La Jolla, CA). After extraction, the RNA was quantified using a UV spectrometer to monitor the absorbance ratio at 260/280 nm. The integrity of the RNA was checked by running the sample in 1% agarose-formaldehyde gels. Samples were maintained at −20°C or −80°C for long-term storage.

### *One-Step RT-PCR*

The RT-PCR reaction was performed using a Stratagene one-step RT-PCR kit. A standard protocol with a 0.6 μM concentration of each primer, 2 μg of template RNA, and the reagent master mix was used to amplify the fragments during the temperature cycles. Control reactions without the RT cycle were performed. To detect the rat MCT mRNA, we used the following set of primers: *1*) MCT1 sense (5′-GTCTACGACCTATGTTGGG-3′) and antisense (5′-CCTCCGCTTTCTGTTCT-3′) to obtain a 320-bp product, *2*) MCT2 sense (5′-GGGGCTGGGTTGTAGT-3′) and antisense (5′-GACGGTGAGGTAAAGTTCTA-3′) to obtain a 296-bp product, *3*) MCT3 sense (5′-CGCTGCTCTAAGAACATCTCATC-3′) and antisense (5′-TCTGGCCTCGTGCCTCAT-3′) to obtain a 238-bp product, and *4*) MCT4 sense (5′-GGCAGTCCCGTGTTCCTTT-3′) and antisense (5′-GCACCTTCTTGAGCCCTGTTAT-3′) to obtain a 421-bp product. Primers were obtained from Life Technologies (custom primers; GIBCO-BRL, Grand Island, NY). cDNA products were separated on a 2% agarose gel, and images were acquired using a Stratagene Eagle Eye II imaging system.

### *MCT Sequences*

All of the MCT sequences were obtained from GenBank. Accession numbers were D63834 (MCT1), X97445 (MCT2), AF059258 (MCT3), and U87627 (MCT4) (12).

### *cDNA Extraction and Sequencing*

PCR products were extracted from the agarose gel using a QIAquick gel extraction kit (Qiagen, Santa Clarita, CA). After extraction, the PCR products were cloned into a TOPO-TA cloning vector (Invitrogen, Carlsbad, CA) according to the manufacturer's instructions. Transformed cells were grown overnight at 37°C, and positive colonies were subcultured in 3 ml of Luria-Bertani medium containing ampicillin. Plasmids were purified using a standard alkaline lysis/polyethylene glycol precipitating protocol and analyzed in a 2% agarose gel after *Eco*RI digestion. Plasmids containing the MCT sequences were sent to the Iowa State University DNA sequencing facility for sequencing.

### *Preparation of RNA Probes*

Probes for in situ hybridization were made with the same sense primers used for RT-PCR. Digoxigenin-UTP-linked probes anti-MCT1 and anti-MCT2 mRNA were prepared using a master mix containing sense primer (35 pmol/μl), digoxigenin-11-2′-deoxyuridine-5′-triphosphate, dATP (9 mM), $CoCl_2$ (5 mM), and terminal deoxynucleotidyl transferase (25 U) for 1 h at 37°C. The probes were stored at −20°C.

### *In Situ Hybridization*

Cells or tissue sections (5 μm) were placed on silane-treated slides and fixed for 10 min with HistoChoice (Amresco, Solon, OH). The slides were then washed three times and left to dry at room temperature. Subsequently, acetone (100%) fixation was performed for 20 min. The slides were stored at −70°C for up to 1 mo. For hybridization, the cell or tissue slides were washed with PBS, treated with β-mercaptoethanol (15 mM, 8 min), and washed again with 2× SCC buffer (300 mM NaCl and 30 mM sodium citrate, pH 7.2). The samples were incubated with the hybridization mixture [0.5 ml of formamide, 100% (GIBCO-BRL); 0.2 ml of 20× SSC; 0.2 ml of dextran sulfate (50%; Sigma); 29 μl of salmon DNA (8.7 mg/ml); 25 μl of yeast transfer RNA (10 mg/ml); 10 μl of 100× Denhardt's solution; 4 μl of EDTA (500 mM); and 32 μl of $H_2O$] for 30 min at 37°C. The hybridization mixture was eliminated without washing, and the samples were incubated overnight with the complete hybridization solution (hybridization mix + probe) at 37°C. The probe dilution was 1:200 in hybridization mixture. For detection purposes, antidigoxigenin Fab coupled to alkaline phosphatase was used (1:500 dilution). The immune reactions were performed using a standard protocol. Substrate solution was composed of 1 μl of levamisole (240 mg/ml), 4.5 μl of nitro blue tetrazolium dye (75 mg/ml), and 3.5 μl of 5-bromo-4-chloro-3-indolyl phosphate (50 mg/ml) in 1 ml of Tris·HCl buffer (in mM: 100 Tris·HCl, 100 NaCl, and 50 $MgCl_2$, pH 9.5). Control experiments were performed using 200× cold probe (sense primer) together with 1× digoxigenin-labeled sense primer.

The samples were histologically mounted on slides, and images were acquired using a Zeiss Axioscope microscope equipped with a Nikon DXM1200 digital camera.

*Immunohistochemistry and Immunocytochemistry of MCT1, MCT2, and MCT4*

Affinity-purified antibodies against MCT1, MCT2, and MCT4 isoforms and the corresponding antigenic peptides were obtained from Alpha Diagnostic International (San Antonio, TX). The expression of MCT1, MCT2, and MCT4 isoforms in rat testes was determined by performing histochemical analysis of thin sections prepared from archived paraffin-embedded tissue blocks according to the method described by Zambrano et al. (41). Paraffin was removed by incubating the sections in xylene followed by absolute alcohol, and it was rehydrated by immersion in graded alcohol solutions. Immunocytochemistry of isolated pachytene spermatocytes and round spermatids was performed on cell smears, similarly to the tissue sections. Endogenous peroxidase was inactivated by treating the tissue sections and cells with 3% $H_2O_2$ for 15 min at room temperature. Sections and cell smears were incubated in PBS containing 5% skim milk, followed by incubation overnight at room temperature with affinity-purified anti-MCT1, anti-MCT2, and anti-MCT4 isoform antibodies (in 1% BSA-PBS), pH 7.4, and 0.3% Triton X-100. Tissue sections and cell smears were washed and incubated with anti-rabbit IgG-horseradish peroxidase (1:100 dilution; Amersham, Arlington Heights, IL) for 2.5 h at room temperature. Immunostaining was performed using 0.05% 3,3′-diaminobenzidine and 0.03% $H_2O_2$. Cells and tissue sections were counterstained with hematoxylin. The antibodies preadsorbed with the respective peptides were used as controls.

*Determination of [$^{14}$C]L-Lactate Flux*

The radioactive flux measurements were performed at 18°C. Approximately 7 million cells/ml were suspended at the different L-lactate concentrations described in RESULTS. [2-$^3$H]-D-Mannitol was added to the cell suspension at a final concentration of 10 μCi/ml. Subsequently, L-[U-$^{14}$C]lactic acid sodium salt was added to the cell suspension at *time 0* at a concentration of 3 μCi/ml. After the desired times had elapsed, 0.5 ml of the cell suspension was layered on top of a dibutylphthalate-dodecane mixture (1 ml; 1.025 g/ml density) in an Eppendorf microcentrifuge tube and centrifuged for 1 min at 15,000 *g*. The supernatant on top of the dibutylphthalate-dodecane layer was removed, and the upper part of the tube was rinsed four times with distilled water. The dibutylphthalate-dodecane mixture was then removed, and the cell pellet was suspended in 250 μl of 0.1 M NaOH and 0.1% Triton X-100. Aliquots of the supernatant and cell pellet suspension were mixed with scintillation liquid and counted in a Beckman 1800 scintillation counter with $^3$H and $^{14}$C counting windows. Intracellular [$^{14}$C]-L-lactate concentration was obtained by correcting for extracellular space trapping in the cell pellet as described previously (30). The concentration of L-lactate entering the cells was calculated using the external specific radioactivity, which was obtained from the supernatant radioactive counts and the external L-lactate concentration.

*Intracellular pH Measurements*

The intracellular pH ($pH_i$) of rat spermatogenic cells was estimated on the basis of fluorescence measurements of intracellular 2′,7′-bis(2-carboxyethyl)-5(6)-carboxyfluorescein (BCECF). Cells were incubated in Krebs-Henseleit (KH)-L-lactate-$Ca^{2+}$ medium with 5 μM BCECF-AM (Molecular Probes, Eugene, OR) for 30 min at room temperature in a 95% $O_2$-5% $CO_2$ atmosphere. After loading the probe, the cells were washed three times and suspended in KH-$Ca^{2+}$ medium. To inhibit the main $H^+$ transport system in spermatids and pachytene spermatocytes (25), dicyclohexyl carboxiimide, a nonspecific $H^+$-ATPase inhibitor, was added to the cells at 18 or 30°C 20 min before the $pH_i$ measurements. The excitation fluorescence ratio of 505/445 nm was determined using an emission wavelength of 535 nm in a Spex FluoroMax-2 fluorometer (HORIBA Jobin Yvon, Edison, NJ). $pH_i$ measurements were performed at a cell density of ~2 million cells/ml. After a basal fluorescence ratio was obtained, different L-lactate concentrations were added to the cell suspension and the fluorescence ratio was recorded until it reached a new steady-state level. Calibration of intracellular BCECF was performed as described by Rink et al. (34). The buffering capacity of spermatogenic cells was determined by measuring $pH_i$ and using $NH_4Cl$ pulses as described by Boron (5), and we found values of 21 ± 7 mM/pH unit ($N$ = 3) and 25 ± 5 mM/pH unit ($N$ = 3) for pachytene spermatocytes and round spermatids, respectively, at pH 7.2.

*$pH_i$ Data Analysis*

Initial velocities of $pH_i$ changes were determined by performing linear regression analysis of the $pH_i$ vs. time records 1 min before and 45 s after L-lactate addition. L-Lactate-dependent $pH_i$ changes were calculated by subtraction of the rates of $pH_i$ changes in the presence and absence of L-lactate, respectively. The rates of L-lactate-dependent $pH_i$ changes at different L-lactate concentrations were corrected by the buffering capacity of the cells on the basis of estimated buffering capacity (see above; see also Ref. 5) and the volume per million cells from the average diameter of round spermatids (11 μm) and pachytene spermatocytes (16 μm). L-Lactate-dependent $H^+$ uptake was expressed as picomolar $H^+$ per minute per million cells.

*Software*

For primer design, we used Primer Premier 5.0 software (Premier Biosoft International, Palo Alto, CA). Alignments were performed using ALN3 software, version 1.1. Images were processed with Adobe Photoshop version 5.5 (Adobe Systems, San Jose, CA) and with TotalLab 1.11 software (Nonlinear Dynamics, Newcastle upon Tyne, UK). $pH_i$ measurement and kinetic data analysis were performed with Microcal Origin software version 5.0 (OriginLab, Northampton, MA). Statistical analysis was performed with GraphPad InStat software, version 3.05 (GraphPad Software, San Diego, CA).

*Chemicals and Isotopes*

L-[U-$^{14}$C]lactic acid sodium salt was obtained from Amersham Pharmacia (Little Chalfont, UK); its specific activity was 152 mCi/mmol. [2-$^3$H]-D-Mannitol was obtained from ICN Biomedicals (Irvine, CA); its specific activity was 20 Ci/mmol. Unless stated otherwise, all other chemicals were obtained from Sigma-Aldrich (St. Louis, MO).

## RESULTS

### *[$^{14}$C]-L-Lactate Transport in Round Spermatids*

Figure 1*A* shows the time course of [$^{14}$C]-L-lactate uptake by rat round spermatids at 18°C. More than 95% of the L-lactate uptake was inhibited by 2 mM α-cyano-4-OH cinnamate (CHC), an inhibitor of MCT-mediated transport (39). In subsequent experiments, 40-s sampling was used to obtain initial velocities of L-lactate uptake in round spermatids. Figure 1*B* shows the relationship between the initial rate of L-lactate uptake by rat round spermatids and the concentrations of L-lactate in the medium in the absence and presence of CHC. These data indicate that L-lactate uptake in these cell was >95% mediated by MCT-mediated transport. At <4 mM external L-lactate concentration, the uptake had a tendency to saturate (see Fig. 1*B*, *inset*). Raising the L-lactate concentration to >4 mM led to an increment in the uptake of this compound by mechanisms that were also inhibited by CHC (Fig. 1*B*). These results strongly suggest that the MCT-mediated L-lactate

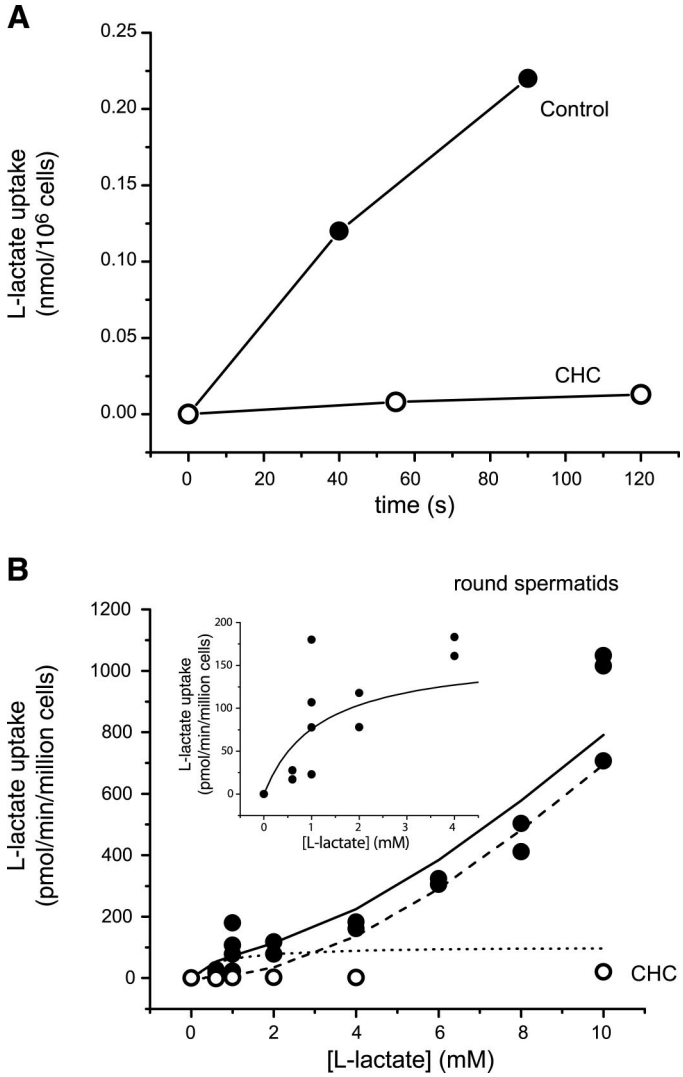


Fig. 1. *A*: [$^{14}$C]-L-lactate uptake in rat round spermatids. Cells in suspension were incubated with 3 μCi/ml radioactive L-lactate and 10 μCi/ml of [2-$^{3}$H]-D-mannitol and 1 mM total L-lactate concentration in the absence and presence of 2 mM α-cyano-4-OH cinnamate (CHC) at 18 ± 1°C. At the indicated times, aliquots of the cell suspension were removed and filtered through a mixture dibutylphthalate-dodecane as described in MATERIALS AND METHODS. The data are expressed as the calculated amount of intracellular L-lactate taken up per million cells. The data shown were obtained from a cell preparation from the testicles of two rats and represent, in terms of the time course of the uptake, measurements performed in two different cell preparations. *B*: [$^{14}$C]-L-lactate uptake in rat round spermatids as a function of extracellular L-lactate concentration. Radioactive L-lactate and mannitol were added at *time 0*, and aliquots were taken 40–45 s later. Other conditions and calculations were as described for *A*. These data represent measurements performed in four different cell preparations obtained from the testicles of two rats for each preparation. The lines represent the theoretical curves obtained for a hyperbola ($V_{max}$ = 150 pmol/min/million cells, $K_m$ = 1.0 mM; dotted line), a sigmoid [$V_{max}$ = 3,100 pmol/min/million cells, $K_{0.5}$ = 27 mM, $n$ = 2 (fixed); dashed line], and the sum of both curves (solid line). The kinetic parameters for each curve were obtained by performing nonlinear fitting of the experimental data at high L-lactate concentration (>4 mM), subtraction of the predicted data at each experimental point at low L-lactate concentration, nonlinear fitting of the resulting data at low L-lactate concentration, and repetition of these rounds of fitting and calculations three times for each range of L-lactate concentrations. *Inset*, uptake data at low L-lactate concentration.

transport was occurring in both high- and low-affinity transport systems. Because of isotope dilution, >10 mM L-lactate concentrations were not tested in these types of measurements, and hence the possible saturation properties of the low-affinity, MCT-mediated transport system were not evident using this experimental strategy. On the basis of the analysis of the L-lactate-dependent $H^+$ transport (see below), we simulated the kinetic behavior of [$^{14}$C]-L-lactate transport using a high-affinity hyperbola, together with a low-affinity sigmoid curve (see solid and dashed lines in Fig. 1*B*). The kinetic parameters in these curves were as follows: hyperbola, $K_m$ 1.0 mM and $V_{max}$ 150 pmol/min/million cells; sigmoid, L-lactate concentration giving half maximal uptake ($K_{0.5}$) 27 mM, $V_{max}$ 3,100, and Hill coefficient ($n_H$) 2 (fixed).

### *L-Lactate Transport Estimated from $pH_i$ Measurements*

*Round spermatids.* Consistent with the [$^{14}$C]-L-lactate transport measurements and with the fact that MCT-mediated trans-

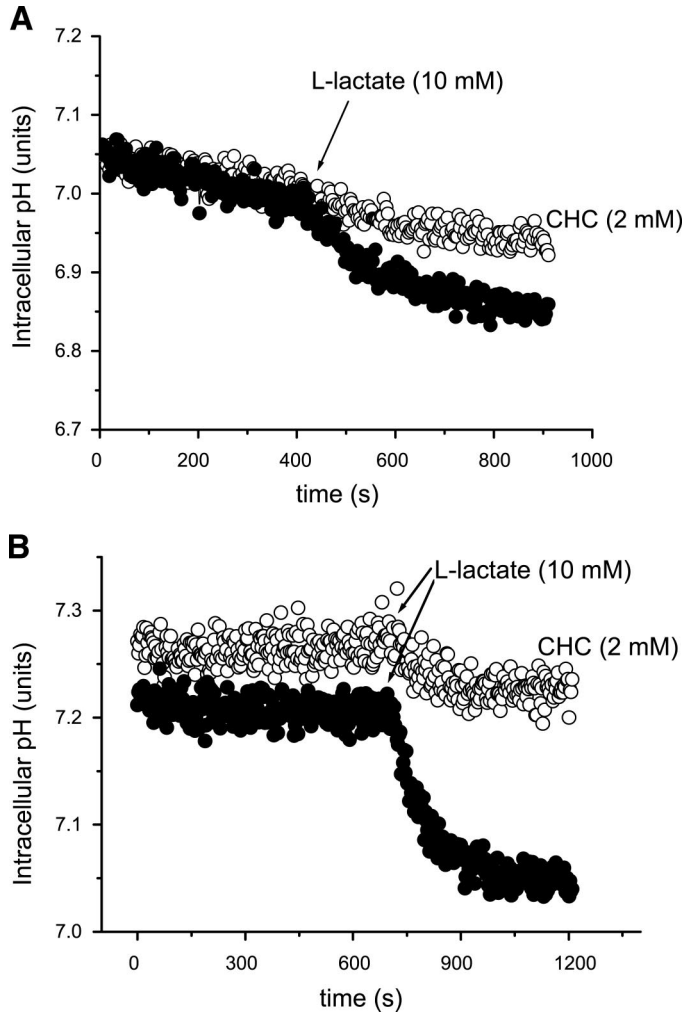


Fig. 2. *A*: intracellular pH ($pH_i$) of round spermatids as a function of time. The cells were incubated for 10 min with dicyclohexyl carboxiimide (DCCD; 50 μM) to inhibit the V-type $H^+$-ATPase in these cells. At the indicated times, 10 mM L-lactate was added in the absence or presence of 2 mM CHC at 18°C. *B*: $pH_i$ of pachytene spermatocytes as a function of time. The cells were incubated for 10 min with DCCD (50 μM) to inhibit the V-type $H^+$-ATPase in these cells. At the indicated times, 10 mM L-lactate was added in the absence or presence of 2 mM CHC at 18°C.

port is an L-lactate-$H^+$ cotransporter, the decrease in $pH_i$ induced by external L-lactate added to a suspension of round spermatids was inhibited by CHC (Fig. 2*A*). To express the data in the same units as those used to express L-lactate uptake, we corrected the L-lactate-dependent $H^+$ uptake data using the average buffering capacity of the cells (see MATERIALS AND METHODS) and the average diameter of round spermatids (11 μm; range, 9–12.5 μm).

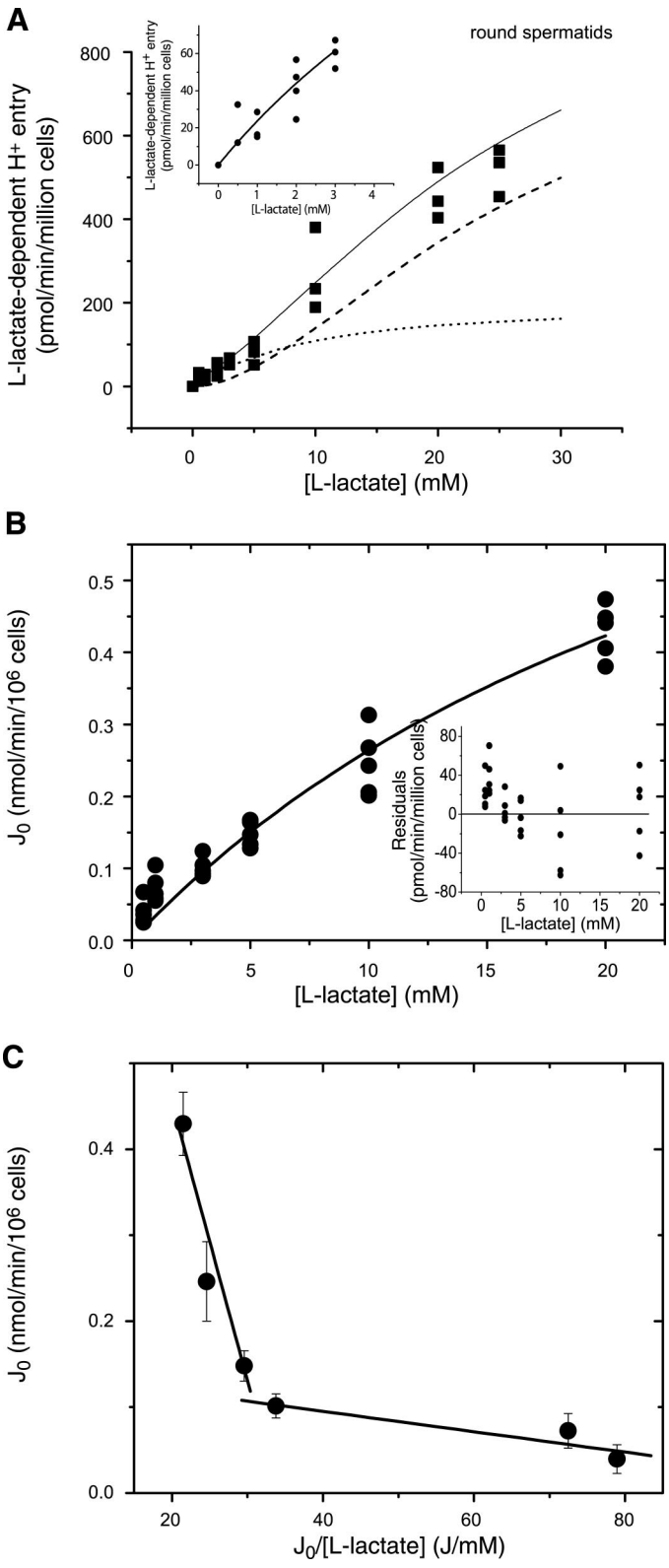


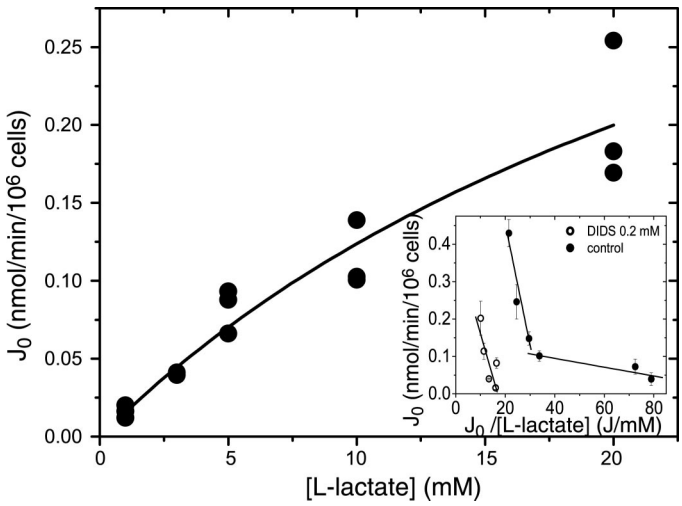


Fig. 4. L-Lactate-dependent rate of $H^+$ entry in rat round spermatids as a function of extracellular L-lactate concentration estimated in the presence of 50 μM DCCD and 0.2 mM 4,4′-diisothiocyanostilbene-2,2′-disulfonic acid (DIDS) at 30°C. The data points shown represent measurements of the initial rate of L-lactate-dependent intracellular acidification performed in at least three different cell preparations obtained from two rats for each preparation. The line represents the theoretical curve obtained for one hyperbola fit of the data. *Inset*, Eadie-Hofstee plot of the data from control experiments (absence of DIDS) and in the presence of DIDS. The kinetic parameters obtained using Eadie-Hofstee linearization were $K_m$ 20 mM and $V_{max}$ 366 pmol/min/million cells.

The graphic representation of the L-lactate-dependent $H^+$ uptake vs. L-lactate concentration data at 18°C suggests an inflexion in the curve at ~3–5 mM external L-lactate (Fig. 3*A*). At 30°C, this inflexion was less evident (Fig. 3*B*). The fit to one hyperbola at both 18 and 30°C led to residuals (experimental value minus the fitted equation predicted value; e.g., Fig. 3*B*, *inset*) showing a strong skewness at low L-lactate concentra-

Fig. 3. *A*: L-lactate-dependent rate of $H^+$ entry in rat round spermatids as a function of extracellular L-lactate concentration in the presence of 50 μM DCCD at 18°C. The data points represent measurements of the initial rate of L-lactate-dependent intracellular acidification performed in at least four different cell preparations obtained from two rats for each preparation. Three of the cell preparations were used to obtain a complete set of data points for low to high L-lactate concentrations. The lines represent the theoretical curves obtained for a hyperbola ($V_{max}$ = 207 pmol/min/million cells, $K_m$ = 8.3 mM; dotted line), a sigmoid ($V_{max}$ = 678 pmol/min/million cells, $K_{0.5}$ = 23 mM, $n$ = 1.7; dashed line), and the sum of both curves (solid line). The kinetic parameters for each curve were obtained by performing nonlinear fitting of the experimental data at high L-lactate concentration (>4 mM), subtraction of the predicted data at each experimental point at low L-lactate concentration, nonlinear fitting of the resulting data at low L-lactate concentration, and repetition of these rounds of fitting and calculations four times for each range of L-lactate concentrations. *Inset*, the uptake data at low L-lactate concentration. *B*: L-lactate-dependent rate of $H^+$ entry in rat round spermatids as a function of extracellular L-lactate concentration in the presence of 50 μM DCCD at 30°C. The data points shown represent measurements of the initial rate of L-lactate-dependent intracellular acidification performed in at least four different cell preparations obtained from two rats for each preparation. The line represents the theoretical curve obtained for one hyperbola fit of the data. *Inset*, residual values (i.e., experimental value minus fitted equation predicted value) for the uptake data. *C*: Eadie-Hofstee plot of the data shown in *B* (30°C). The values obtained for the hyperbolas were as follows: high affinity, $K_m$ 1.2 mM and $V_{max}$ 142 pmol/min/million cells; low affinity, $K_m$ 33.4 mM and $V_{max}$ 1,117 pmol/min/million cells.

tions, suggesting that a one-hyperbola model was not adequate to describe the data. On the basis of the sigmoidicity of L-lactate transport reported by Beaudry et al. (2) in muscle cells, we fitted the data at 18°C to a sigmoid curve (Hill model). An analysis of residuals after the sigmoid fitting strongly suggested that a second function was needed at low L-lactate concentrations. Beaudry et al. (2) also presented a similar positive skewness of the residuals at low L-lactate concentrations when fitted to a Hill model. Thus neither one hyperbola nor one sigmoid model was able to describe our L-lactate transport data adequately. At 18°C, an Eadie-Hofstee or Hanes-Woolf linearization of the L-lactate-dependent $H^+$ uptake did not present either a one- or a two-hyperbola linearization or a classical sigmoid inflexion (data not shown; see Ref. 37). Thus we present the data at 18°C fitted with a high-affinity hyperbola and a lower-affinity sigmoid (Hill) curve, taking into account that this mixed curve seems to reproduce better the tendency of our experimental data and that

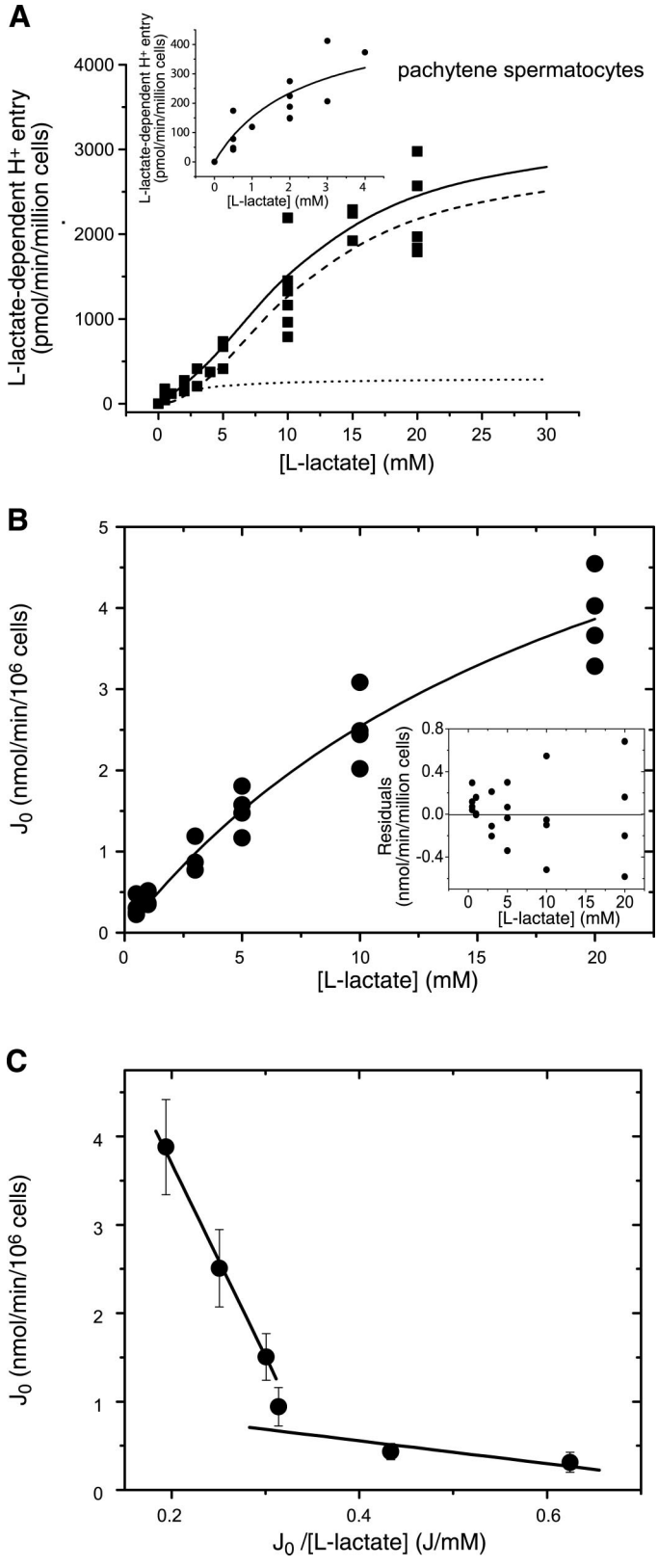


Fig. 5. *A*: L-Lactate-dependent rate of $H^+$ entry in rat pachytene spermatocytes as a function of extracellular L-lactate concentration in the presence of 50 μM DCCD at 18°C. The data points shown represent measurements of the initial rate of L-lactate-dependent intracellular acidification performed in at least four different cell preparations obtained from two rats for each preparation. The lines represent the theoretical curves obtained for a hyperbola ($V_{max}$ = 409 pmol/min/million cells, $K_m$ = 2.4 mM; dotted line), a sigmoid ($V_{max}$ = 2,802 pmol/min/million cells, $K_{0.5}$= 10.8 mM, $n$ = 2.1; dashed line), and the sum of both curves (solid line). The kinetic parameters for each curve were obtained as described for Fig. 3*A*. *Inset*, uptake data at low L-lactate concentration. *B*: L-lactate-dependent rate of $H^+$ entry in rat pachytene spermatocytes as a function of extracellular L-lactate concentration estimated in the presence of 50 μM DCCD at 30°C. The data points shown represent measurements of the initial rate of L-lactate-dependent intracellular acidification performed in at least four different cell preparations obtained from two rats each for each preparation. The line represents the theoretical curve obtained for one hyperbola fit of the data. *Inset*, the residuals (experimental value minus fitted equation predicted value) for the uptake data. *C*: Eadie-Hofstee plot of the data shown in *B* (30°C). The values obtained for the hyperbolas were high affinity, $K_m$ 1.9 mM and $V_{max}$ 1,431 pmol/min/million cells, and low affinity, $K_m$ 22.3 mM and $V_{max}$ 8,165 pmol/min/million cells.

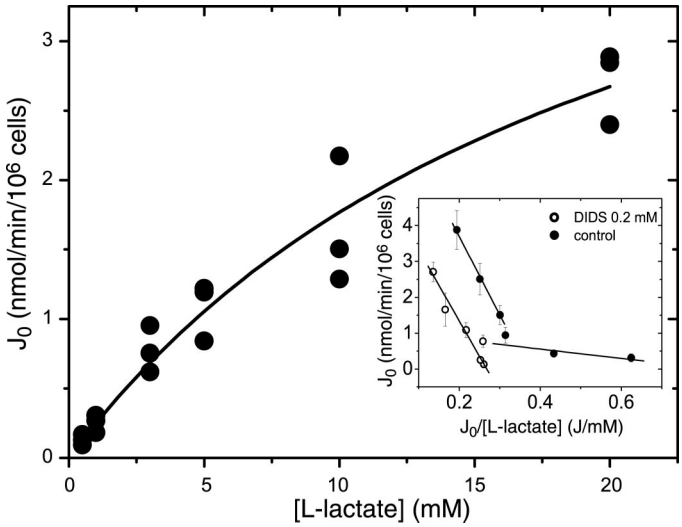


Fig. 6. L-Lactate-dependent rate of $H^+$ entry in rat round spermatids as a function of extracellular L-lactate concentration estimated in the presence of 50 μM DCCD and 0.2 mM DIDS at 30°C. The data points shown represent measurements of the initial rate of L-lactate-dependent intracellular acidification performed in at least three different cell preparations obtained from two rats for each preparation. The line represents the theoretical curve obtained for one hyperbola fit of the data. *Inset*, Eadie-Hofstee plot of the data in control experiments (absence of DIDS) and in the presence of DIDS. The kinetic parameters obtained from Eadie-Hofstee linearization were $K_m$ 17.4 mM and $V_{max}$ 4,835 pmol/min/million cells.

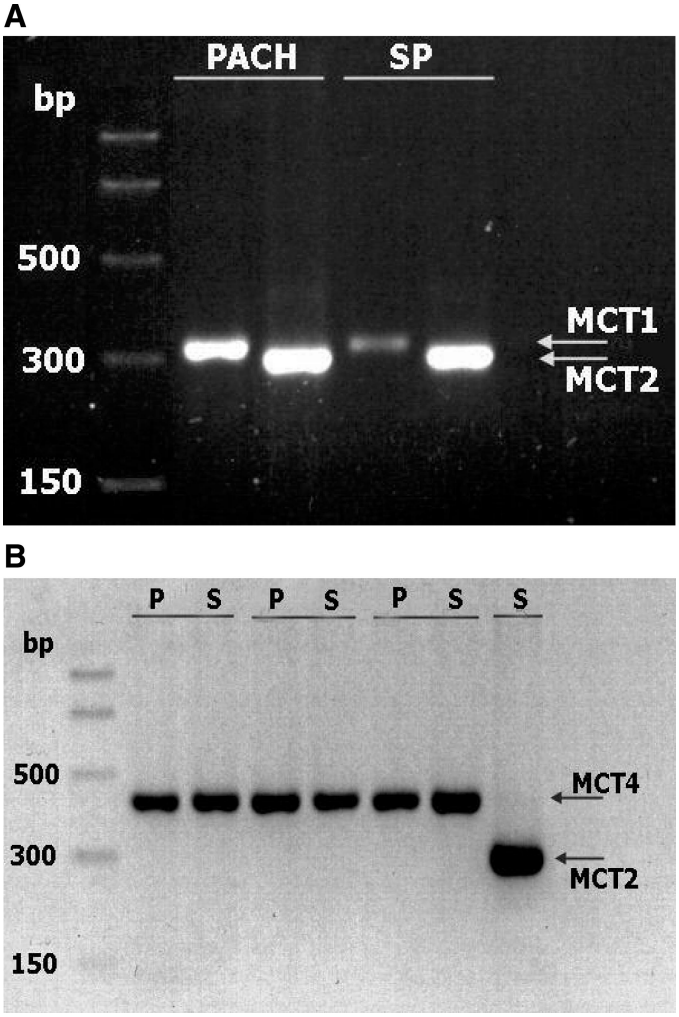


Fig. 7. *A*: agarose gel electrophoresis of RT-PCR products for MCT1 (320 bp) and MCT2 (296 bp) isoforms obtained from round spermatids (sp) and pachytene spermatocytes (pach). These data are representative of similar results obtained in three different cell preparations. *B*: agarose gel electrophoresis of RT-PCR products for MCT4 (421 bp) isoforms obtained from round spermatids (s) and pachytene spermatocytes (p) in three different cell preparations. The datum shown for MCT2 was obtained in the last preparation and is shown for comparison purposes.

the Beaudry et al. (2) data showed similar kinetic behavior of L-lactate uptake in a similar multitransporter system. The kinetic parameters for the high-affinity hyperbola and the sigmoid curve were obtained from a nonlinear fit of the experimental data at low L-lactate concentration (<4 mM), subtraction of the predicted data at each experimental point at high L-lactate concentration, and subsequent repetition of these calculations three times for each range of L-lactate concentrations (see, e.g., Ref. 38). At 18°C, we obtained the following values for the kinetic parameters: high affinity, $K_m$ 8.3 mM and $V_{max}$ 207 pmol/min/million cells; low affinity (Hill model), $K_{0.5}$ 23 mM, $V_{max}$ 678 pmol/min/million cells, and $n_H$ 1.7. The parameters obtained for the low-affinity component presented relatively larger errors that were most likely derived from the scatter of the data at L-lactate concentrations >10 mM, the L-lactate concentrations used (below $K_m$), and the more stringent statistical requirements to fit the low-affinity sigmoid curve.

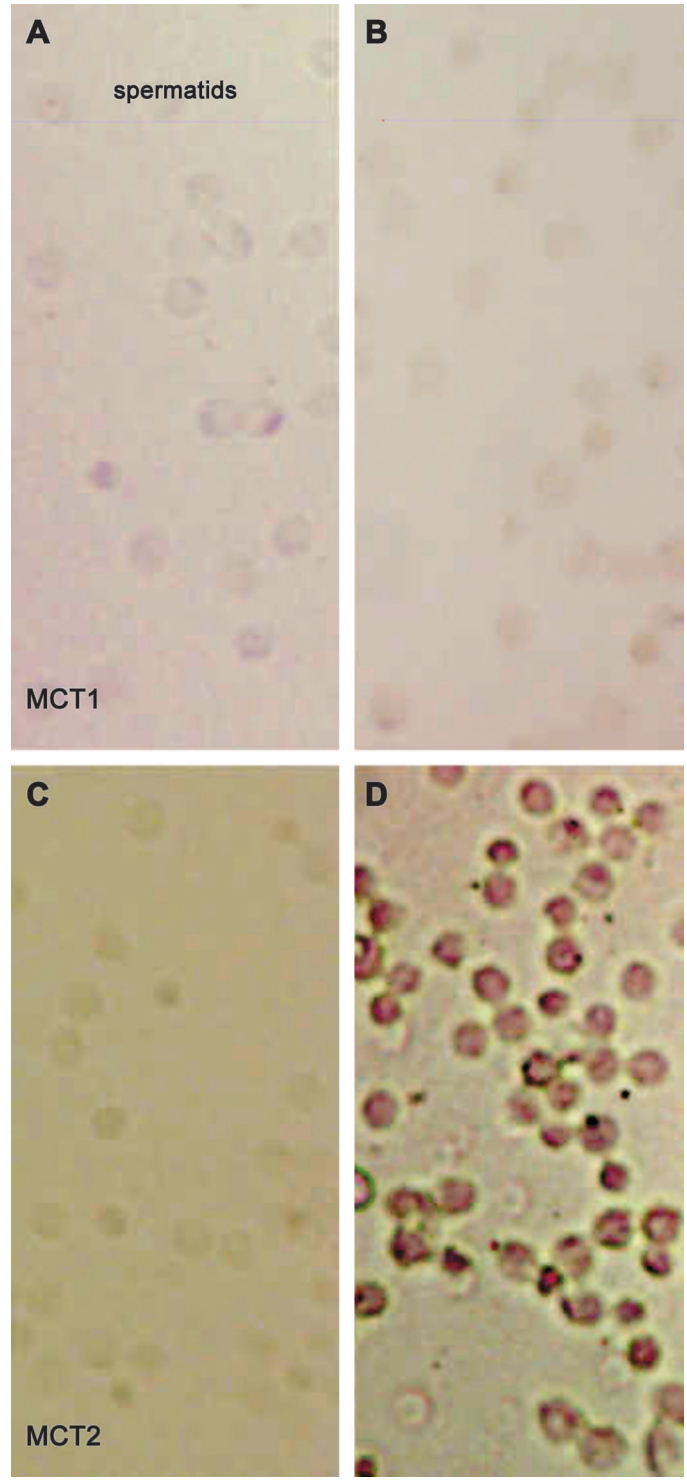


Fig. 8. In situ hybridization of MCT1 (*A* and *B*) and MCT2 (*C* and *D*) transcripts in rat round spermatids, as well as digoxigenin-UTP-linked probes anti-MCT1 and anti-MCT2 mRNA (*B* and *D*), are shown. For detection purposes, anti-digoxigenin Fab coupled to alkaline phosphatase was used. Control experiments were performed using 200× unlabeled probe (sense primer), together with 1× digoxigenin-labeled sense primer (*A* and *C*). Technique is described in MATERIALS AND METHODS.

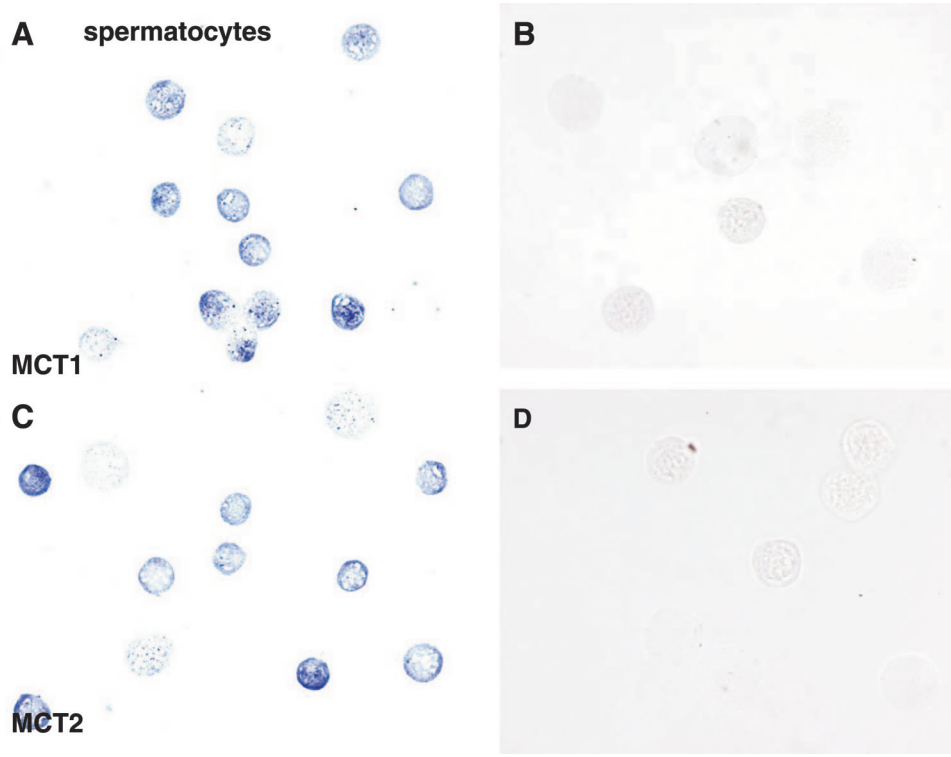


Fig. 9. In situ hybridization of MCT1 (*A* and *B*) and MCT2 (*C* and *D*) transcripts in rat pachytene spermatocytes. Digoxigenin-UTP-linked probes anti-MCT1 and anti-MCT2 mRNA. For detection purposes, antidigoxigenin Fab coupled to alkaline phosphatase was used. Control experiments were performed using 200× unlabeled probe (sense primer), together with 1× digoxigenin-labeled sense primer (*B* and *D*). Technique is described in MATERIALS AND METHODS.

At 30°C, a Hanes-Woolf or Eadie-Hofstee representation of the data showed high- and low-affinity components (Fig. 3*C*). At 30°C, the kinetic parameters for high- and low-affinity hyperbolas were obtained using the Eadie-Hofstee linearization method. At this temperature, we obtained the following values for the kinetic parameters: high affinity, $K_m$ 1.2 ± 0.5 mM and $V_{max}$ 142 ± 34 pmol/min/million cells; low affinity, $K_m$ 33.4 ± 10.5 mM and $V_{max}$ 1,117 ± 268 pmol/min/million cells.

It is known that 4,4′-diisothiocyanostilbene-2,2′-disulfonic acid (DIDS) seems to inhibit MCT1 and MCT2, but not MCT4 (29). Consistent with this property of DIDS, this compound produced a partial inhibition of L-lactate-dependent $H^+$ uptake in round spermatids at 30°C (see Fig. 4). Eadie-Hofstee analysis of the DIDS-insensitive component of this uptake (Fig. 4, *inset*) showed that it was well described by a single component that presented the kinetic parameters $K_m$ 20 ± 9 mM and $V_{max}$ 366 ± 127 pmol/min/million cells. Thus DIDS was able to differentiate, and at the same time corroborated, that round spermatids have at least two components of L-lactate transport kinetically corresponding to what has been described as L-lactate transport mediated by high-affinity MCT (MCT1 and/or MCT2) and low-affinity MCT4.

*Pachytene spermatocytes.* Pachytene spermatocytes also showed L-lactate-dependent $H^+$ entry inhibited by CHC at 18°C (Fig. 2*B*). To express the data in the same units as those used to measure the L-lactate uptake, we corrected the L-lactate-dependent $H^+$ uptake data using the average buffering capacity of the cells (see MATERIALS AND METHODS) and the average diameter of pachytene spermatocytes (16 μm; range, 14–18 μm). Similarly to L-lactate entry in round spermatids at 18°C, the kinetic data showed a shoulder ~5 mM L-lactate, suggesting the operation of more than one transport system for this compound (Fig. 5*A*). The data were analyzed similarly to the data obtained for spermatids (see above). We obtained the following kinetic parameters at 18°C: high affinity, $K_m$ 2.35 mM and $V_{max}$ 409 pmol/min/million cells; low affinity (sigmoid), $K_{0.5}$ 10.8 mM, $V_{max}$ 2,802 pmol/min/million cells, and $n_H$ 2.1.

We obtained the following values for the kinetic parameters at 30°C (Fig. 5, *B* and *C*): high affinity, $K_m$ 1.9 ± 1.0 mM and $V_{max}$ 1,431 ± 462 pmol/min/million cells; low affinity $K_m$ 22.3 ± 1.2 and $V_{max}$ 8,165 ± 293 pmol/min/million cells.

Similarly to the findings for round spermatids, DIDS was able to inhibit partially the L-lactate-dependent $H^+$ uptake in pachytene spermatocytes (Fig. 6). The Eadie-Hofstee analysis of the DIDS-insensitive component of this uptake showed that it was well described by a single component that presented the kinetic parameters $K_m$ 17.4 ± 2.7 mM and $V_{max}$ 4,835 ± 586 pmol/min/million cells.

### *Different Isoforms of MCT in Spermatogenic Cells*

The L-lactate transport measurements indicated that L-lactate entered both pachytene spermatocytes and round spermatids using MCT transporters. Furthermore, our kinetic data strongly suggest that at least two different transport systems for L-lactate were present in both pachytene spermatocytes and round spermatids. Thus, to test the hypothesis of a differentiation of MCT expression during the meiotic-postmeiotic transition in spermatogenesis, we studied the expression of the MCT1, MCT2, MCT3, and MCT4 transcripts in pachytene spermatocytes and round spermatids using RT-PCR. Figure 7, *A* and *B*, shows the pattern of agarose gel electrophoresis of the RT-PCR products for MCT1, MCT2, and MCT4. We did not find any detectable expression of MCT3 in pachytene spermatocytes or round spermatids. The RT-PCR products pre-

sented the expected number of bases for the MCT1, MCT2, and MCT4 amplification products. Furthermore, sequencing of the RT-PCR products showed that their aligned sequences were 100% identical to the sequences flanked by the primers designed. Simultaneous RT-PCR for MCT1 consistently showed a less strong signal in round spermatids than in pachytene spermatocytes (Fig. 7*A*). MCT2 and MCT4 expression did not show obvious differences between cell types (Fig. 7, *A* and *B*).

### *In Situ Hybridization of MCT Isoforms in Spermatogenic Cells and Seminiferous Tubules*

Our RT-PCR data of MCT isoforms in pachytene spermatocytes and round spermatids suggest that MCT1 was decreased in round spermatids. Thus, to test directly for the presence of the MCT1 and MCT2 transcripts in spermatogenic cells, we performed in situ hybridization to MCT1 and MCT2 mRNA in pachytene spermatocytes and round spermatids. Figure 8, *A* and *C*, shows the control in situ hybridization performed in the presence of excess unlabeled probes for MCT1 and MCT2, respectively, in round spermatids. Figure 8, *B* and *D*, shows the hybridization with digoxigenin-labeled probes for MCT1 and MCT2, respectively, in round spermatids. These images show that MCT1 transcripts were not detected using this technique in round spermatids. In contrast, pachytene spermatocytes showed positive staining for both MCT1 and MCT2 (Fig. 9, *A* and *C*, respectively; controls, Fig. 9, *B* and *D*).

### *Immunohistochemistry and Immunocytochemistry for MCT1, MCT2, and MCT4 in Rat Testis and Spermatogenic Cells*

Expression of the MCT1, MCT2, and MCT4 isoforms at the protein level in rat round spermatids and pachytene spermatocytes is shown in Figures 10, *A–F*, and 11, *A–F*, respectively. It can be shown that pachytene spermatocytes expressed the MCT1 and MCT4 isoforms, but the expression of MCT2 was less evident. In fact, MCT2 immunoreactivity in pachytene spermatocytes demonstrated faint localization to what is likely the Golgi apparatus in the cell. Round spermatids showed strong MCT1 immunoreactivity but weaker immunoreactivity for MCT2 and MCT4. These data observed with isolated cells were corroborated with seminiferous tubule sections, which are shown in Fig. 12. MCT1 immunoreactivity was observed in the

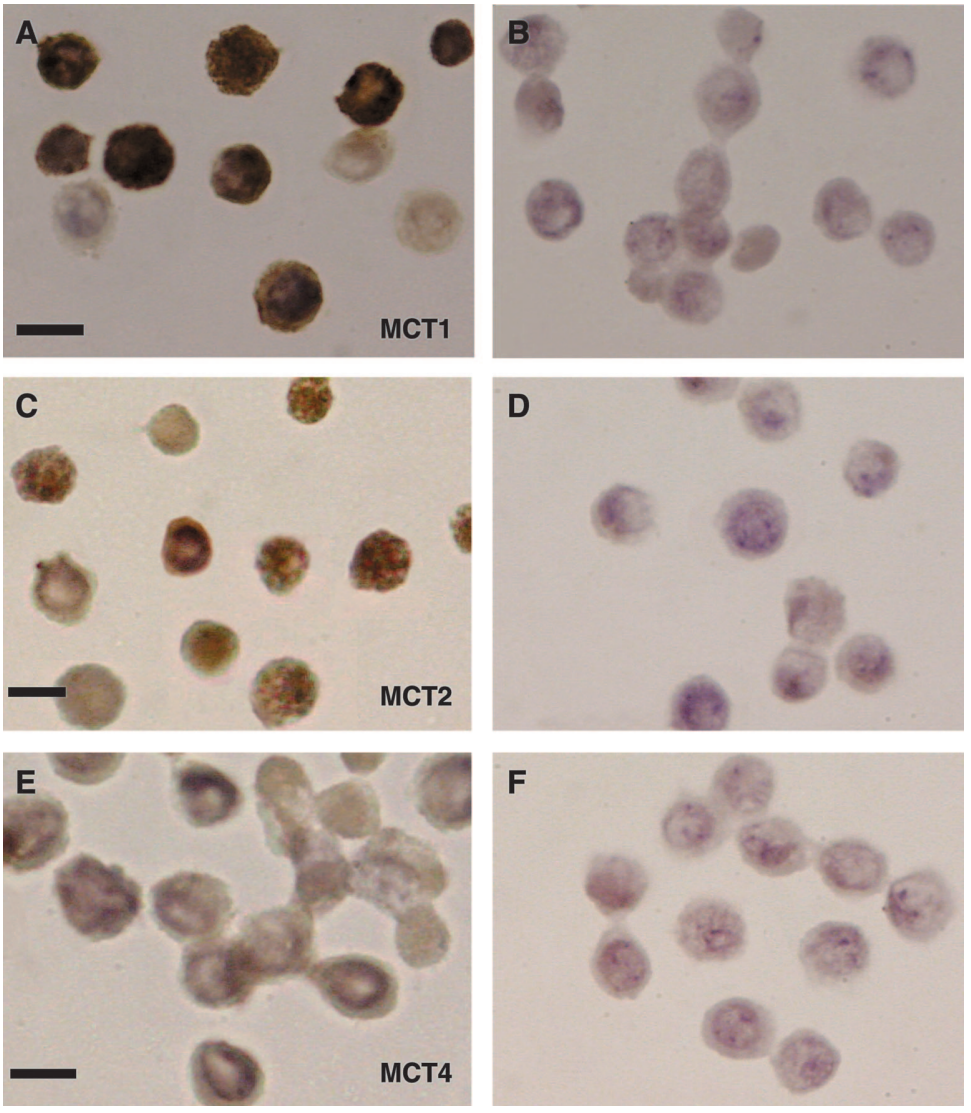


Fig. 10. Immunocytochemistry performed for MCT1, MCT2, and MCT4 in isolated round spermatids. Affinity-purified rabbit antibodies against MCT1, MCT2, and MCT4 isoforms were used. Anti-rabbit IgG-horseradish peroxidase was used as secondary antibody, and immunoassay was performed using 0.05% 3,3′-diaminobenzidine and 0.03% $H_2O_2$. Cells were counterstained with hematoxylin. Images at *left* and *right*, respectively, represent the immunoassays for round spermatids without and with preadsorption of the antibody with the corresponding antigenic peptides. Immunoreactions for MCT1 (*top*), MCT2 (*middle*), and MCT4 (*bottom*). Bar, 10 μm.

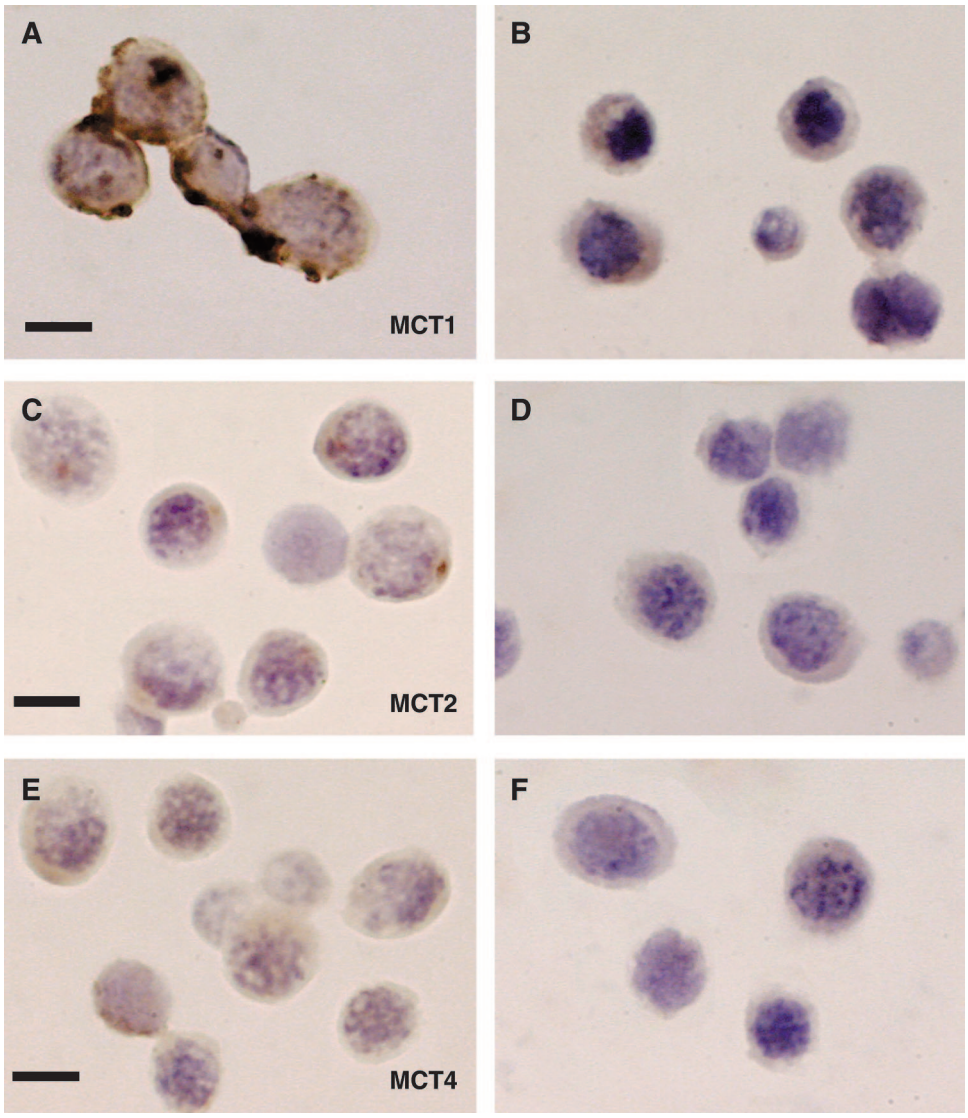


Fig. 11. Immunocytochemistry performed for MCT1, MCT2, and MCT4 in isolated pachytene spermatocytes. Affinity-purified rabbit antibodies against MCT1, MCT2, and MCT4 isoforms were used. Anti-rabbit IgG-horseradish peroxidase was used as a secondary antibody, and immunoassay was performed using 0.05% 3,3′-diaminobenzidine and 0.03% $H_2O_2$. Cells were counterstained with hematoxylin. Images at *left* and *right*, respectively, represent the immunoassays for round spermatids without and with preadsorption of the antibody with the corresponding antigenic peptides. Immunoreactions for MCT1 (*top*), MCT2 (*middle*), and MCT4 (*bottom*). Bar, 10 μm.

interstitial cells and also in surrounding spermatogenic cells in the seminiferous tubules. A MCT2-related histochemical reaction was strongly observed in interstitial cells as well as on the tails of spermatozoa in the lumina of the tubules (see also Ref. 6), with a weaker reaction observed in seminiferous tubule cells. A strong MCT4-related histochemical reaction was observed in interstitial cells, with a weaker reaction observed in seminiferous tubule cells.

## DISCUSSION

L-Lactate transport is a key element in metabolic communication between tissues (e.g., Cori cycle; see also Ref. 26) and cells (e.g., glial cell-neuron interaction; see also Ref. 19). Four MCT isoforms (i.e., L-lactate) have been described in rodents. MCT3 is expressed mainly in the retina (27). A postulated L-lactate export role has been proposed for MCT4 on the basis of its expression in highly glycolytic cells (9). Expression of MCT1 and MCT2 is more widespread, and low $K_m$ values for MCT1 and MCT2 transport suggest that their role might be related to L-lactate uptake from the external environment of the cells (13).

As noted in the introductory text, the metabolic properties of spermatogenic cells suggest that they can either export glycolytic L-lactate or take up L-lactate from the medium, depending on the availability of glucose and L-lactate in the external environment. The environmental availability of L-lactate and glucose is controlled by the hormonally regulated glycolytic activity of Sertoli cells, which are the sustentacular cells in the seminiferous epithelium. Hence, transport and metabolism of these metabolic substrates would be part of the signals connecting the physiological activities of these different cell types.

In the present study, we have found that L-lactate-$H^+$ transport properties of spermatogenic cells, which show at least two components of L-lactate transport, are in agreement with the expression of MCT4 (a low-affinity/high-capacity transport system), together with MCT1 (intermediate affinity) and/or MCT2 (high affinity) in pachytene spermatocytes and round spermatids. The expression of these isoforms and the differentiation of the expression of MCT1 and MCT2 at the spermatid stages of spermatogenic cell development were confirmed by our RT-PCR results and in situ hybridization. The cytochemistry of MCT1, MCT2, and MCT4 showed that MCT1 was

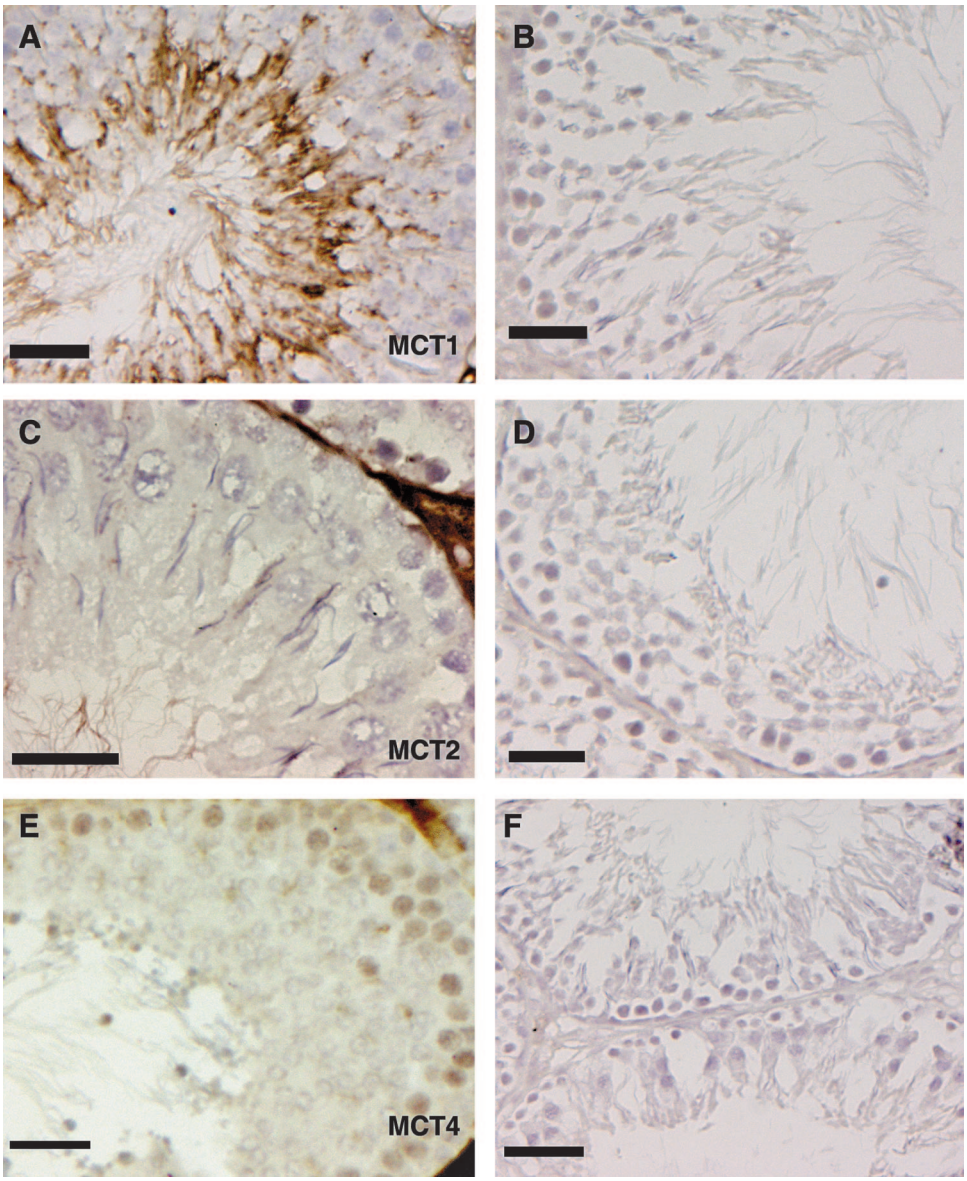


Fig. 12. Immunohistochemistry for MCT1, MCT2, and MCT4 in testicular sections. Affinity-purified rabbit antibodies against MCT1, MCT2, and MCT4 isoforms were used. Anti-rabbit IgG-horseradish peroxidase was used as a secondary antibody, and immunostaining was performed using 0.05% 3,3′-diaminobenzidine and 0.03% $H_2O_2$. Tissue sections were counterstained with hematoxylin. At *left* and *middle*, respectively, are shown low- and high-magnification light transmission microscopic immunostaining images, respectively. *Right* image shows control immunostaining, in which the antibodies were preadsorbed with the respective peptides. Immunoreactions for MCT1 (*top*), MCT2 (*middle*) and MCT4 (*bottom*). Bar, 20 μm.

present in pachytene spermatocytes and in round spermatids. MCT2 was weakly evident at the protein level in pachytene spermatocytes and apparently was intracellularly localized, even though the RNA transcript was clearly detected. MCT4 was present in both cell types at both the mRNA and protein levels. These data are in agreement with our kinetic data suggesting the existence of at least two components of L-lactate transport in these cells, consisting of both high-affinity/low-capacity and low-affinity/high-capacity L-lactate uptake of this monocarboxylate transporter. The tendency to saturate at ~5 mM, followed by a further increase in uptake at higher L-lactate concentrations, was reproducible in our experiments with pachytene spermatocytes and round spermatids. In oocytes and when expressed alone, MCT4-mediated transport does not show sigmoid kinetics (20). However, in differentiated muscle cells that contained both high- and low-affinity MCT transport systems, Beaudry et al. (2) showed that, similarly to spermatogenic cells, a sigmoid relationship between L-lactate uptake and L-lactate concentration was obtained. The mechanism of this sigmoid relationship between L-lactate uptake and L-lactate concentration is not well understood. However, it has been shown that MCT1 and MCT4 can be regulated by expression of and interaction with CD70 and CD147, a family of plasma membrane glycoproteins (8). Furthermore, it was recently demonstrated that coexpression of MCT1 and the $Na^+$-$HCO_3^-$ transporter in oocytes can induce activation of MCT1 through a $pH_i$-related mechanism, strongly suggesting that complex kinetic behavior can be expected in cells expressing several isoforms of MCT and other acid-base transporters (3).

The evidence that the high-affinity isoform L-lactate transporter MCT2 shows greater expression at the protein level in round spermatids strongly suggests that this isoform has a role in or is a consequence of cell differentiation in the spermatogenic process. The fact that L-lactate can maintain low $[Ca^{2+}]_i$ with $K_{0.5}$ of ~0.7 mM (32) suggests, first, that MCT1 and MCT2 transport capacity is adequate to supply reducing equivalents to the mitochondria to maintain physiological levels of intracellular ATP (and activity of transport ATPases) in these cells and, second, that MCT4 appears to play a role in these cells that is not related to the entry of L-lactate into oxidative metabolism.

Our results are consistent with the idea that spermatogenic cells differentially express L-lactate transporter isoforms that could allow coordination of metabolism and $[Ca^{2+}]_i$ (32) by the hormonally regulated metabolic and transport activity of Sertoli cells. This metabolic signaling from Sertoli cells could be coupled to spermatogenic cell metabolism, channeling glycolytic L-lactate toward MCT4 and external L-lactate toward MCT1 or MCT2 and cell mitochondrial oxidative metabolism. This working hypothesis describes an integrated physiological role for the experimentally observed spermatogenic, cell metabolic, and membrane transport differentiation, which has remained puzzling thus far (see, e.g., Ref. 10).


## ACKNOWLEDGMENTS

We thank Drs. Lee Anne McLean and Cathy Fuller for kind help and instruction with RT-PCR of MCT isoforms. We also thank Monica Brito for instructing S. Brauchi with regard to in situ hybridization techniques.

## GRANTS

This work was supported by El Fondo Nacional de Desarrollo Científico y Tecnológico Grant 1990398, Vicerrectoría de Investigación y Estudios Avanzados of the Pontificia Universidad Católica de Valparaíso DI 125.751, and National Institute of Diabetes and Digestive and Kidney Diseases Grant DK-37206.


## REFERENCES


1. **Bajpai M, Gupta G, and Setty BS.** Changes in carbohydrate metabolism of testicular germ cells during meiosis in the rat. *Eur J Endocrinol* 138: 322–327, 1998.
2. **Beaudry M, Mouaffak N, el Abida K, Rieu M, and Mengual R.** Lactate transport in L6 skeletal muscle cells and vesicles: allosteric or multisite mechanism and functional membrane marker of differentiation. *Acta Physiol Scand* 162: 33–46, 1998.
3. **Becker HM, Bröer S, and Deitmer JW.** Facilitated lactate transport by MCT1 when coexpressed with the sodium bicarbonate cotransporter (NBC) in *Xenopus* oocytes. *Biophys J* 86: 235–247, 2004.
4. **Bonen A, Tonouchi M, Miskovic D, Heddle C, Heikkila JJ, and Halestrap AP.** Isoform-specific regulation of the lactate transporters MCT1 and MCT4 by contractile activity. *Am J Physiol Endocrinol Metab* 279: E1131–E1138, 2000.
5. **Boron WF.** Control of intracellular pH. In: *The Kidney: Physiology and Pathophysiology* (2nd ed.), edited by Seldin DW and Giebisch G. New York: Raven, 1992, vol. 1, p. 219–263.
6. **Boussouar F, Mauduit C, Tabone E, Pellerin L, Magistretti PJ, and Benahmed M.** Developmental and hormonal regulation of the monocarboxylate transporter 2 (MCT2) expression in the mouse germ cells. *Biol Reprod* 69: 1069–1078, 2003.
7. **Bröer S, Rahman B, Pellegri G, Pellerin L, Martin JL, Verleysdonk S, Hamprecht B, and Magistretti PJ.** Comparison of lactate transport in astroglial cells and monocarboxylate transporter 1 (MCT 1) expressing *Xenopus laevis* oocytes: expression of two different monocarboxylate transporters in astroglial cells and neurons. *J Biol Chem* 272: 30096–30102, 1997.
8. **Buyse M, Sitaraman SV, Liu X, Bado A, and Merlin D.** Luminal leptin enhances CD147/MCT-1-mediated uptake of butyrate in the human intestinal cell line Caco2-BBE. *J Biol Chem* 277: 28182–28190, 2002.
9. **Dimmer KS, Friedrich B, Lang F, Deitmer JW, and Bröer S.** The low-affinity monocarboxylate transporter MCT4 is adapted to the export of lactate in highly glycolytic cells. *Biochem J* 350: 219–227, 2000.
10. **Gladden LB.** Lactate metabolism: a new paradigm for the third millennium. *J Physiol* 558: 5–30, 2004.
11. **Goddard I, Florin A, Mauduit C, Tabone E, Contard P, Bars R, Chuzel F, and Benahmed M.** Alteration of lactate production and transport in the adult rat testis exposed in utero to flutamide. *Mol Cell Endocrinol* 206: 137–146, 2003.
12. **Grootegoed JA, Jansen R, and van der Molen HJ.** Effect of glucose on ATP dephosphorylation in rat spermatids. *J Reprod Fertil* 77: 99–107, 1986.
13. **Halestrap AP and Price NT.** The proton-linked monocarboxylate transporter (MCT) family: structure, function and regulation. *Biochem J* 343: 281–299, 1999.
14. **Hall PF and Mita M.** Influence of follicle-stimulating hormone on glucose transport by cultured Sertoli cells. *Biol Reprod* 31: 863–869, 1984.
15. **Herrera E, Salas K, Lagos N, Benos DJ, and Reyes JG.** Energy metabolism and its linkage to intracellular $Ca^{2+}$ and pH regulation in rat spermatogenic cells. *Biol Cell* 92: 429–440, 2000.
16. **Jegou B.** The Sertoli-germ cell communication network in mammals. *Int Rev Cytol* 147: 25–96, 1993.
17. **Jutte NHPM, Grootegoed JA, Rommerts FFG, and van der Molen HJ.** Exogenous lactate is essential for metabolic activities in isolated rat spermatocytes and spermatids. *J Reprod Fertil* 62: 399–405, 1981.
18. **Le Gac F, Attramadal M, Borrebaek B, Horn R, Froysa A, Tvermyr M, and Hansson V.** Effects of FSH, isoproterenol, and cyclic AMP on the production of lactate and pyruvate by cultured Sertoli cells. *Arch Androl* 10: 149–154, 1983.
19. **Magistretti PJ and Pellerini L.** Astrocytes couple synaptic activity to glucose utilization in the brain. *News Physiol Sci* 14: 177–182, 1999.
20. **Manning Fox JE, Meredith D, and Halestrap AP.** Characterisation of human monocarboxylate transporter 4 substantiates its role in lactic acid efflux from skeletal muscle. *J Physiol* 529: 285–293, 2000.
21. **Mita M and Hall PF.** Metabolism of round spermatids from rats: lactate as the preferred substrate. *Biol Reprod* 26: 445–455, 1982.
22. **Nakamura M, Fujiwara A, Yasumasu I, Okinaga S, and Arai K.** Regulation of glucose metabolism by adenine nucleotides in round spermatids from rat testis. *J Biol Chem* 257: 13945–13950, 1982.
23. **Nakamura M, Okinaga S, and Arai K.** Studies of metabolism of round spermatids: glucose as an unfavorable substrate. *Biol Reprod* 35: 927–935, 1986.
24. **Nakamura M, Yamaguchi K, Suzuki A, Okinaga S, and Arai K.** Metabolism of round spermatids: a possible regulation of hexose transport. *Dev Growth Differ* 28: 499–504, 1986.
25. **Osses N, Pancetti F, Benos DJ, and Reyes JG.** Intracellular pH regulation in rat round spermatids. *Biol Cell* 89: 273–283, 1997.
26. **Perriello G, Jorde R, Nurjhan N, Stumvoll M, Dailey G, Jenssen T, Bier DM, and Gerich JE.** Estimation of glucose-alanine-lactate-glutamine cycles in postabsorptive humans: role of skeletal muscle. *Am J Physiol Endocrinol Metab* 269: E443–E450, 1995.
27. **Philp NJ, Yoon H, and Lombardi L.** Mouse MCT3 gene is expressed preferentially in retinal pigment and choroid plexus epithelia. *Am J Physiol Cell Physiol* 280: C1319–C1326, 2001.
28. **Poole RC and Halestrap AP.** Reversible and irreversible inhibition, by stilbenedisulphonates, of lactate transport into rat erythrocytes: identification of some new high-affinity inhibitors. *Biochem J* 275: 307–312, 1991.
29. **Poole RC and Halestrap AP.** Interaction of the erythrocyte lactate transporter (monocarboxylate transporter 1) with an integral 70-kDa membrane glycoprotein of the immunoglobulin superfamily. *J Biol Chem* 272: 14624–14628, 1997.
30. **Reyes JG, Arrate MP, Santander M, Guzman L, and Benos DJ.** Zn(II) transport and distribution in rat spermatids. *Am J Physiol Cell Physiol* 265: C893–C900, 1993.
31. **Reyes JG, Diaz A, Osses N, Opazo C, and Benos DJ.** On stage single cell identification of rat spermatogenic cells. *Biol Cell* 89: 53–66, 1997.
32. **Reyes JG, Herrera E, Lobos L, Salas K, Lagos N, Jorquera RA, Labarca P, and Benos DJ.** Dynamics of intracellular calcium induced by lactate and glucose in rat pachytene spermatocytes and round spermatids. *Reproduction* 123: 701–710, 2002.
33. **Reyes JG, Velarde MV, Ugarte R, and Benos DJ.** The glycolytic component of rat spermatid energy and acid-base metabolism. *Am J Physiol Cell Physiol* 259: C660–C667, 1990.
34. **Rink TJ, Tsien RY, and Pozzan T.** Cytoplasmic pH and free $Mg^{2+}$ in lymphocytes. *J Cell Biol* 95: 189–196, 1982.
35. **Robinson R and Fritz IB.** Metabolism of glucose by Sertoli cells in culture. *Biol Reprod* 24: 1032–1041, 1981.
36. **Romrell LJ, Bellvé AR, and Fawcett DW.** Separation of mouse spermatogenic cells by sedimentation velocity: a morphological characterization. *Dev Biol* 49: 119–131, 1976.
37. **Segel IH.** *Enzyme Kinetics: Behavior and Analysis of Rapid Equilibrium and Steady State Enzyme Systems*. New York: Wiley, 1975.
38. **Spears G, Sneyd JGT, and Loten EG.** A method for deriving kinetic constants for two enzymes acting on the same substrate. *Biochem J* 125: 1149–1151, 1971.
39. **Spencer TL and Lehninger AL.** L-Lactate transport in Ehrlich ascites-tumour cells. *Biochem J* 154: 405–414, 1976.
40. **Turner TT, D'Addario DA, and Howards SS.** The transepithelial movement of $^3$H-3-*O*-methyl-D-glucose in the hamster seminiferous and caudal epididymal tubules. *Fertil Steril* 40: 530–535, 1983.
41. **Zambrano A, Noli C, Rauch MC, Werner E, Brito M, Amthauer R, Slebe JC, Vera JC, and Concha II.** Expression of GM-CSF receptors in male germ cells and their role in signaling for increased glucose and vitamin C transport. *J Cell Biochem* 80: 625–634, 2001.